Received: 24 April 2023 | Revised: 8 June 2023 | Accepted: 10 June 2023

DOI: 10.1002/hyp.14930

RESEARCH ARTICLE

WILEY

Evaluating the effects of stream power on rill flow resistance

Alessio Nicosia[1] | Vincenzo Pampalone[1] | Maria Angela Serio[1] | Vito Ferro[1,2]

[1]Department of Agricultural, Food and Forest Sciences, University of Palermo, Palermo, Italy

[2]NBFC, National Biodiversity Future Center, Palermo, Italy

Correspondence
Alessio Nicosia, Department of Agricultural, Food and Forest Sciences, University of Palermo, Viale Delle Scienze, Building 4, 90128 Palermo, Italy.
Email: alessio.nicosia@unipa.it

Abstract

Limited information is currently available on how sediment transport affects rill flow resistance and the influence of hydraulic variables, as stream power, on sediment transport capacity for rill flows. In this paper, the available measurements of hydraulic variables (flow depth, channel slope, mean flow velocity, Reynolds number, Froude number, and Darcy–Weisbach friction factor) carried out by Ban et al. (Measurement of rill and ephemeral gully flow velocities and their model expression affected by flow rate and slope gradient. *Journal of Hydrology*, 589, 125172) and Ban (Measurements and estimation of flow velocity in mobile bed rills. *International Journal of Sediment Research*, 38(1), 97–104) for fixed and mobile bed rills are used to test the applicability of a theoretically deduced rill flow resistance equation based on a power-velocity profile. The results allowed for stating that (i) the theoretical flow resistance approach can predict Darcy–Weisbach friction factor for flows over fixed and mobile beds, (ii) the stream power, dependent on flow discharge and slope, determines different flow behaviour, and (iii) the data are supportive of the slope independence hypothesis of rill velocity, for the mobile bed condition, only for the highest investigated discharge values (greater than 0.133 L s^{-1}).

KEYWORDS
fixed bed rills, flow resistance, mobile bed rills, soil erosion, transport capacity

1 | INTRODUCTION

Rill erosion is one of the most relevant processes affecting soils due to the significant amount of eroded and transported soil particles (Borrelli et al., 2017; Di Stefano et al., 2022a). According to Govers et al. (2007), rills are narrow, concentrated flow pathways where water depth h and mean flow velocity V exceed those of overland flow. As a result, more flow energy is available for the detachment, entrainment, and transport of soil particles, which increases soil erosion rates (Wirtz et al., 2010). Moreover, rills also receive runoff and sediments delivered from interrill areas (Bagarello & Ferro, 2004; Peng et al., 2015), working as both sediment sources and sediment delivery systems for erosion on hillslopes (Nearing et al., 1997).

The interaction between detached bed material and actual sediment transport determines how rill erosion develops (Wang et al., 2015). The sediment transport capacity T_c, that is, the maximum equilibrium sediment load that flow can transport in a given hydraulic condition, is a hydraulic variable that is significantly influenced by stream power $SP = \tau V$ (Ferro, 1998), where τ is the bottom shear stress, and affects the soil detachment rate and the actual sediment transport. Therefore, the rill flow-sediment transport interaction affects flow resistance and mean velocity and, as a consequence, the flow transport capacity T_c.

The effects of hydraulic variables on the sediment transport capacity have been studied by several authors. Govers (1990), performing an experimental investigation with fine well-sorted quartz mixtures and rill slope s in the range $1.7 \le s \le 21\%$, concluded that T_c

is strictly related to the bottom shear stress and the effective stream power $\Omega = SP^{3/2}/R^{2/3}$, in which R is the hydraulic radius. Everaert (1991) demonstrated that sediment grain size affects the effect of rainfall on sediment transport capacity. For fine sediment, rainfall influence is not significant, while, for coarse sediment, the difference in the transport capacity of undisturbed and disturbed flows depends on the effective stream power. The results obtained by Ferro (1998) confirmed the ability of Ω to be used as a predictor of sediment transport capacity of rainfall-disturbed overland flow suggested by the study of Everaert (1991). Also, Ali et al. (2013) conducted flume experimental runs and derived a new function, based on unit stream power (i.e., the product of slope by mean flow velocity (Yang, 1972)), to quantify transport capacity for overland flows.

The slope effect on flow transport capacity should be affected by the condition of erodible or non-erodible beds, that are characterized by different roughness (Everaert, 1991; Govers, 1990; Zhang et al., 2009). According to previous investigations (Ali et al., 2013; Wu et al., 2016) on flow transport capacity performed for slopes steeper than 17%–18%, the relationships for estimating T_c designed for the gentle slope condition (<18%) should not be applied for steep slopes (>18%).

For $s \geq 18\%$, Peng et al. (2015) conducted flow measurements for supercritical conditions and transitional or turbulent flow regimes and found a significant variation with the slope gradient of the relationship between the Darcy–Weisbach friction factor f and the Reynolds number $Re = Vh/\nu_k$, where ν_k is the water kinematic viscosity. For $s \geq 18\%$, Di Stefano et al. (2021), analysing fixed and mobile bed rill data characterized by a wide range of hydraulic conditions, plot/flume slope (18%–84%) and soil texture (clay ranging from 3% to 71%), demonstrated that flow resistance is affected by the soil texture, representing particle detachability and transportability. For all the investigated conditions, these authors also stated that the Darcy–Weisbach friction factor is linearly related to the rill slope, confirming the occurrence of the 'feedback mechanism' (i.e., the flow velocity tends to be independent of slope) (Govers, 1992). Nicosia et al. (2022), using measurements performed in mobile and fixed bed rills on plots with different slopes (9%, 14%, 15%, 18%, 22%, 24%, 25%, and 26%) and soil textures (clay fractions ranging from 32.7% to 73%), and flume measurements available in the literature, demonstrated that the effect of sediment transport on rill flow resistance differs for gentle and steep slopes. In detail, they found that distinguishing between the steep and gentle slope conditions and calibrating a specific equation for each of them guarantees better estimate performances of the Darcy–Weisbach friction factor. These results led to the conclusion that the distinction between gentle and steep slopes should be made using a slope threshold of 18%.

As obtained for open-channel flows (Gao & Abrahams, 2004), Di Stefano, Nicosia, Pampalone, et al. (2019), analysing the fixed bed data by Jiang et al. (2018), established that flow resistance increases with slope and Shields number, which is a variable representing the effect of bed-load transport. The findings obtained by Di Stefano, Nicosia, Palmeri, et al. (2019) and Di Stefano, Nicosia, Pampalone, et al. (2019) also highlighted that the feedback mechanism did not occur due to the fixed bed conditions in which the cross-section geometry does not change. Further studies about the effects of suspended sediment transport on flow resistance (Di Stefano et al., 2020) led to the conclusion that, for large-size mixtures, they can be neglected, while, for small-size mixtures, the flow resistance decreases for increasing mean sediment concentrations. Moreover, Di Stefano, Nicosia, Palmeri, et al. (2019) and Di Stefano et al. (2022a, 2022b), comparing the results obtained for mobile and fixed bed rills, demonstrated that the effect of the overall sediment transport (i.e., bed load and suspended load) on the rill flow resistance is significantly less substantial than that caused by grain roughness.

Recently, experimental runs on fixed bed rills and clear flow were carried out by Ban et al. (2020) while experiments on mobile bed rills were performed by Ban (2023). Ban et al. (2020) found that the flow velocity fitted well with unit width flow discharge and slope gradient by a power function, leading to a more reliable model as compared to that predicting flow velocity as a function of only flow discharge. For flow discharge less than 0.133 L s^{-1}, Ban (2023) obtained that flow velocity does not depend on the slope while slope gradient combined with a higher flow discharge contributes to better velocity prediction. According to Ban (2023), following the hypothesis of the feedback mechanism (Govers, 1992), for $Q > 0.133$ L s^{-1} the roughness increase directly dissipates flow energy and reduces flow velocity, but cannot completely counterbalance the increase of flow velocity due to steep slope effect. In other words, for $Q > 0.133$ L s^{-1}, the flow velocity is a slope gradient- and flow rate-dependent parameter.

In this paper, the rill flow hydraulic variables (flow depth h, channel slope s, mean flow velocity V, Reynolds number Re, Froude number F, and Darcy–Weisbach friction factor f) corresponding to fixed and mobile bed rills investigated by Ban et al. (2020) and Ban (2023) are used to test the applicability of a theoretically deduced rill flow resistance equation (Ferro, 2018) based on a power-velocity profile. The main aims of this article are (i) testing the theoretical approach using fixed and mobile bed rill data available in the literature, (ii) discussing the effects of flow discharge and slope, governing the stream power, on sediment transport capacity, and (iii) testing the occurrence of the feedback mechanism presented by Govers (1992).

2 | MATERIALS AND METHODS

2.1 | Available dataset

Ban et al. (2020) performed laboratory experiments on flume strips (0.40 m wide, 12 m long, and 0.5 m deep), which were filled with experimental soil (25.62% sand, 64.57% silt, and 9.81% clay) to a depth of 0.4 m and a bulk density of about 1.3 g cm^{-3}. For each strip, a rill, 0.05 m deep and 0.1 m wide, was dug along the central line. The soil surface of the shaped rectangular rills was paved by sandpapers glued with soil particles to obtain a fixed-bed experimental condition. The experiments were carried out for nine sediment-free flow rates (0.017, 0.033, 0.067, 0.133, 0.267, 0.533, 1.067, 2.133, and 4.267 L s^{-1}), and five slope gradients (8.7%, 17.6%, 26.8%, 36.4%, and 46.6%). The flow velocity was measured by the dye tracer technique using a saturated potassium chloride solution as an electrolyte.

Ban (2023) conducted mobile bed rill measurements using the same soil and experimental setup as Ban et al. (2020). The simulated

rills were manually dug to rectangular dimensions (0.10 m wide, 12.00 m long, and 0.10 m deep), and their soil surface was scratched with a wood board to simulate the roughness of natural soil. The experiments were carried out for four slope gradients (8.7%, 17.6%, 26.8%, and 36.4%) and the same nine sediment-free flow rates, in the range 0.017–4.267 L s^{-1}, used by Ban et al. (2020). The water depth values were calculated as $h = Q/Vw$, where w is the channel width.

2.2 | The theoretical flow resistance equation

Although rills and fluvial channels differ significantly, process-oriented soil erosion models use classical hydraulic equations designed for streams/rivers, such as Manning, Darcy–Weisbach, and Chezy's equations (Nicosia & Ferro, 2023; Nouwakpo et al., 2016; Strohmeier et al., 2014). In principle, the integration of a known flow-velocity distribution in the cross-section allows deducing a theoretical flow-resistance law (Ferro & Porto, 2018). For this reason, linking velocity distribution and flow resistance continues to be one of the main challenges for uniform open channel flow hydraulics.

The vertical velocity profile of a uniform turbulent open-channel flow can be represented as (Barenblatt, 1979, 1987; Carollo et al., 2021):

$$\frac{v}{u_*} = \Gamma\left(\frac{u_* y}{\nu_k}\right)^{\delta}, \tag{1}$$

where v is the local velocity, y is the distance from the bottom, $u_* = \sqrt{gRs}$ is the shear velocity, where g is the gravitational acceleration, Γ is a function estimated by velocity measurements, and δ is an exponent calculated as follows (Castaing et al., 1990):

$$\delta = \frac{1.5}{\ln Re}. \tag{2}$$

The Darcy–Weisbach friction factor f follows by integrating Equation (1) (Ferro & Porto, 2018):

$$f = 8\left[\frac{(\delta+1)(\delta+2)}{2^{1-\delta}\Gamma Re^{\delta}}\right]^{2/(1+\delta)}. \tag{3}$$

Setting $y = \alpha\ h$ the distance from the bottom where the local velocity is equal to V, the following equation can be obtained from Equation (1) (Ferro, 2017):

$$\Gamma_v = \frac{V}{u_*\left(\frac{u_* \alpha h}{\nu_k}\right)^{\delta}}, \tag{4}$$

where Γ_v is the Γ value obtained by the measurements of V, R, h, and s, α is a coefficient, dependent on δ (Ferro, 2017) and less than 1, which accounts for the circumstances that V occurs below the water surface and only one velocity profile represents the velocity distribution for the whole cross-section.

The coefficient α has to be calculated by the following theoretical relationship deduced by Ferro (2017):

$$\alpha = \left[\frac{2^{1-\delta}}{(\delta+1)(\delta+2)}\right]^{1/\delta}. \tag{5}$$

Given that Ferro (2018) demonstrated that Γ theoretically depends only on the channel slope, Reynolds number, and Froude number, Γ_v can be estimated by the following equation (Di Stefano et al., 2021; Li et al., 2022; Nicosia et al., 2022):

$$\Gamma_v = a\frac{F^b}{s^c Re^e}, \tag{6}$$

in which $F = V/\sqrt{gh}$ and a, b, c, and e are coefficients estimated by the available measurements.

3 | RESULTS

3.1 | Analysis of mobile bed measurements

For this condition, the measurements of Reynolds and Froude numbers correspond to laminar, transitional, and turbulent flow regimes ($133 \le Re \le 33\,479$) and, with a single exception, to supercritical flows ($0.77 < F \le 3.85$) (Figure 1a).

The 36 measurements carried out by Ban (2023) were used to calibrate Equation (6) obtaining:

$$\Gamma_v = 1.2468\frac{F^{0.5311}Re^{0.0465}}{s^{0.3838}}, \tag{7}$$

characterized by a coefficient of determination R^2 equal to 0.82. Figure 2a shows the comparison between the measured Γ_v values, obtained by Equation (4), and those calculated by Equation (7). By coupling Equation (3) with Equation (7), the following flow resistance equation is obtained:

$$f = 8\left[\frac{(\delta+1)(\delta+2)}{2^{1-\delta}4.4817}\right]^{\frac{2}{1+\delta}}\left[\frac{s^{0.3838}}{1.2468F^{0.5311}Re^{0.0465}}\right]^{\frac{2}{1+\delta}}. \tag{8}$$

Figure 2b shows the comparison between the measured f values and those calculated by Equation (8), which is characterized by a RMSE of 0.0164. The errors in the f estimate falling within the error bands of ±20% and ± 10% are equal to 86.1% and 50%, respectively. Considering that δ varies within a narrow range (0.144–0.306), its mean value (0.208) can be introduced into Equation (8), which becomes:

$$f = 0.9476\frac{s^{0.6354}}{F^{0.8793}Re^{0.0771}}. \tag{9}$$

Ban (2023) observed that rills tended to be slightly eroded for $Q \le 0.133$ L s^{-1}, while they were evidently eroded for

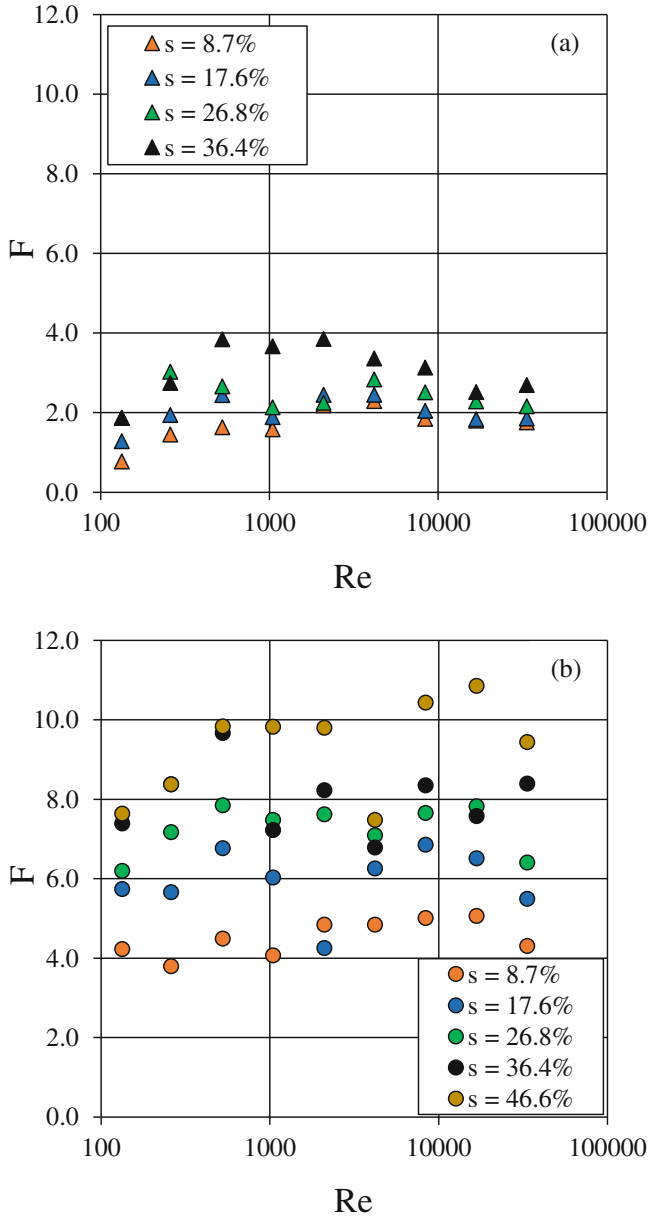

FIGURE 1 Relationship between Froude and Reynolds number for mobile (a) and fixed (b) bed experiments.

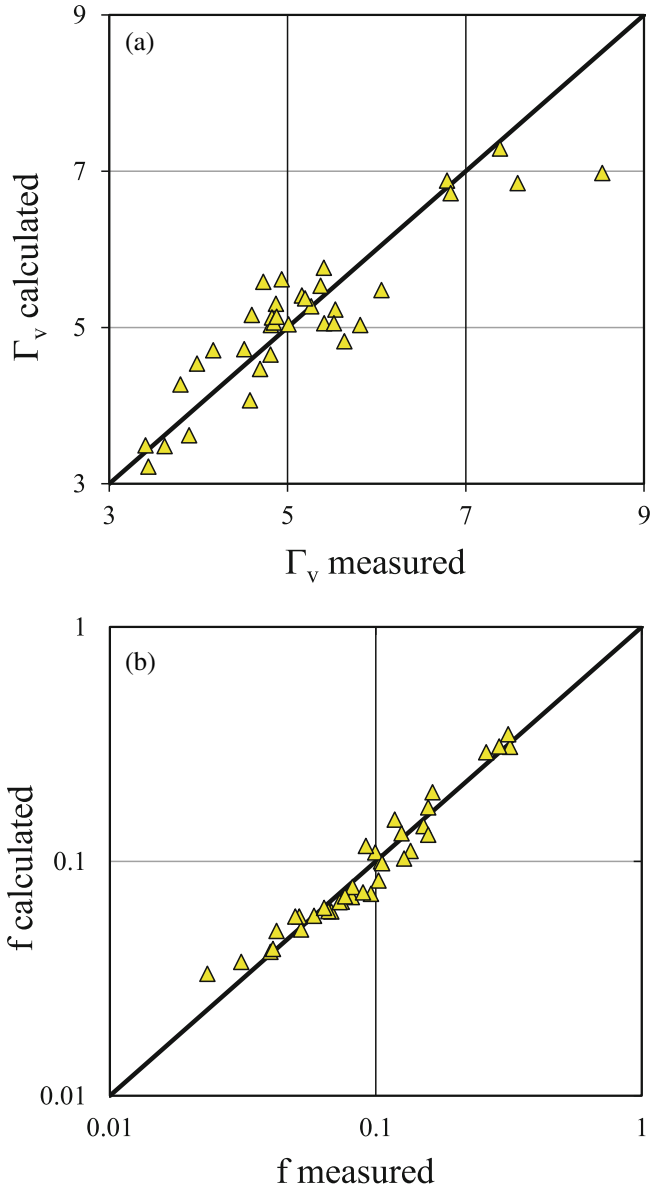

FIGURE 2 Comparison between the measured Γ_v values, obtained by Equation (4), and those calculated by Equation (7) (a), and between the measured f values and those calculated by Equation (8) (b), for all the mobile bed data.

$Q > 0.133$ L s^{-1}. Moreover, this author found the slope independence of flow velocity for Q values under this threshold. The different erosive phenomena observed by Ban (2023) can depend on different ranges of stream power and, consequently, the sediment transport capacity. In fact, high values of flow discharge and slope gradient determine high SP (Figure 3) and T_c, which results in more evident erosive phenomena. Figure 3 shows that a threshold of $Q = 0.133$ L s^{-1} can be used to divide the database as it determines two tendentially distinguished stream power ranges.

Therefore, the calibration of Equation (6) was conducted by splitting the complete dataset into two sub-dataset characterized by $Q \le 0.133$ L s^{-1} (16 data) and $Q > 0.133$ L s^{-1} (20 data), leading to:

$$\Gamma_v = 1.9978 \frac{F^{0.7842}}{s^{0.4375} Re^{0.0757}} \quad (Q \le 0.133\,\mathrm{L\,s} - 1), \tag{10a}$$

$$\Gamma_v = 0.3492 \frac{F^{0.7665} Re^{0.1391}}{s^{0.5212}} \quad (Q > 0.133\,\mathrm{L\,s} - 1), \tag{10b}$$

which are characterized by R^2 equal to 0.973 and 0.971, respectively. Figure 4a shows the comparison between the measured Γ_v values, obtained by Equation (4), and those calculated by Equations (10). By coupling Equation (3) with Equations (10) and considering that Re^{δ} is equal to 4.4817, the following flow resistance equations are obtained:

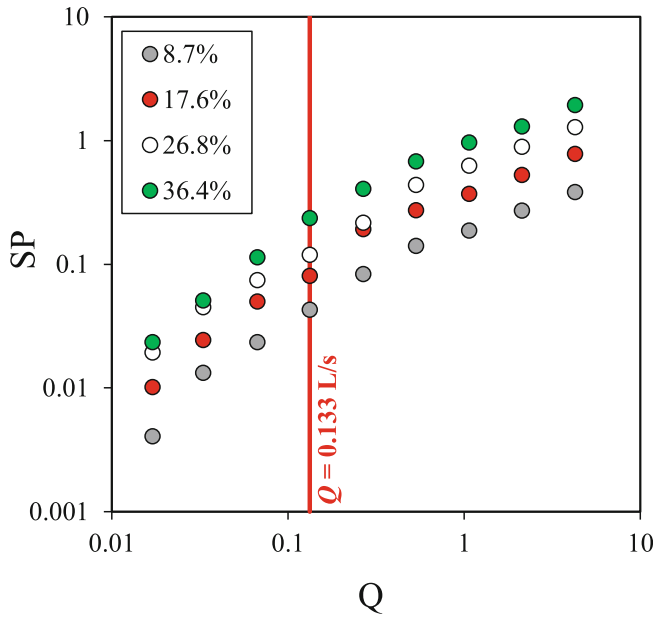

FIGURE 3 Relationship between flow discharge Q and stream power SP for mobile bed rills.

$$f = 8\left[\frac{(\delta+1)(\delta+2)}{2^{1-\delta}4.4817}\right]^{\frac{2}{1+\delta}}\left[\frac{s^{0.4375}Re^{0.0757}}{1.9978F^{0.7842}}\right]^{\frac{2}{1+\delta}} \quad (Q \le 0.133\,\mathrm{L\,s^{-1}}), \quad (11a)$$

$$f = 8\left[\frac{(\delta+1)(\delta+2)}{2^{1-\delta}4.4817}\right]^{\frac{2}{1+\delta}}\left[\frac{s^{0.5212}}{0.3492F^{0.7665}Re^{0.1391}}\right]^{\frac{2}{1+\delta}} \quad (Q > 0.133\,\mathrm{L\,s^{-1}}). \quad (11b)$$

Figure 4b shows the comparison between the measured f values and those calculated by Equations (11), which are characterized by RMSE equal to 0.0063. Distinguishing the data by a discharge threshold, the errors in the f estimate falling within the error bands of ±20% and ±10% are equal to 100% and 94%, respectively. Introducing the δ mean value (0.208) into Equations (11), they become:

$$f = 0.569\frac{s^{0.6956}Re^{0.1203}}{F^{1.2469}} \quad (Q \le 0.133\,\mathrm{L\,s^{-1}}), \quad (12a)$$

$$f = 6.7934\frac{s^{0.8924}}{F^{1.3125}Re^{0.2382}} \quad (Q > 0.133\,\mathrm{L\,s^{-1}}). \quad (12b)$$

3.2 | Analysis of fixed bed measurements

The experiments by Ban et al. (2020) were performed for Reynolds and Froude numbers corresponding to laminar, transitional, and turbulent flow regimes ($133 \le Re \le 33\,479$) and supercritical flows ($3.8 < F \le 10.85$) (Figure 1b).

The 45 fixed bed measurements were used to calibrate Equation (6), obtaining:

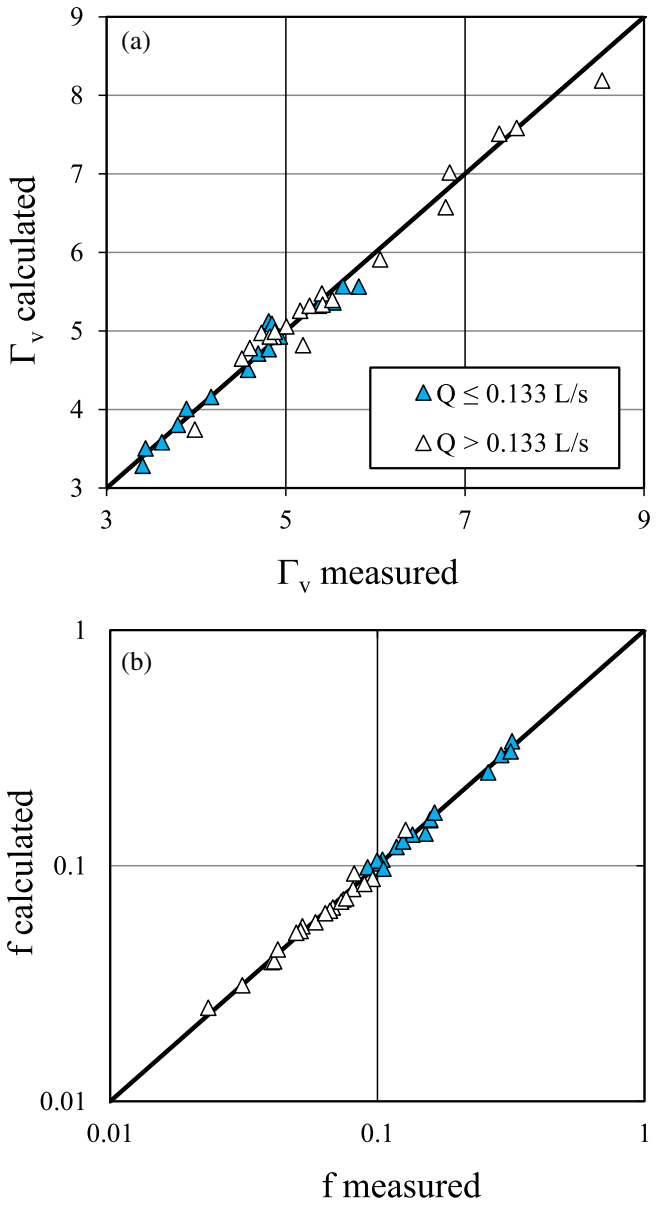

FIGURE 4 Comparison, for the mobile bed rills, between the measured Γ_v values, obtained by Equation (4), and those calculated by Equation (10a), and between the measured f values and those calculated by Equation (11b), distinguishing the data by the threshold $Q = 0.133$ L s^{-1}.

$$\Gamma_v = 1.1971\frac{F^{1.0343}}{s^{0.5435}Re^{0.102}}, \quad (13)$$

which is characterized by R^2 equal to 0.9. Figure 5a shows the comparison between the measured Γ_v values, obtained by Equation (4), and those calculated by Equation (13). For the fixed bed rill condition, by coupling Equation (3) with Equation (13) and considering that Re^{δ} is equal to 4.4817, the following flow resistance equation is obtained:

$$f = 8\left[\frac{(\delta+1)(\delta+2)}{2^{1-\delta}4.4817}\right]^{\frac{2}{1+\delta}}\left[\frac{s^{0.5435}Re^{0.102}}{1.1971F^{1.0343}}\right]^{\frac{2}{1+\delta}}. \quad (14)$$

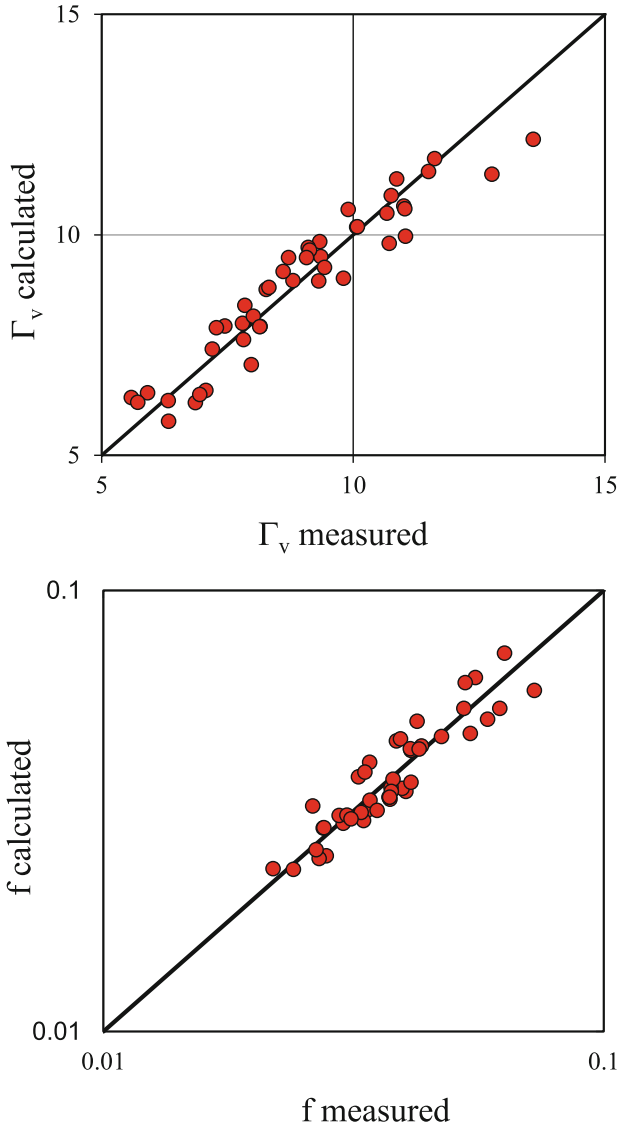

FIGURE 5 Comparison between the measured Γ_v values, obtained by Equation (4), and those calculated by Equation (13) (a), and between the measured f values and those calculated by Equation (14) (b), for all the fixed bed data.

Figure 5b shows the comparison between the measured f values and those calculated by Equation (14), which is characterized by RMSE equal to 0.0048. The errors in the f estimate falling within the error bands of ±20% and ± 10% are equal to 97.8% and 55.56%, respectively. Considering the narrow range of δ (0.144–0.306), its mean value (0.208) can be introduced into Equation (14), which becomes:

$$f = 1.0137 \frac{s^{0.8998} Re^{0.1689}}{F^{1.7125}}. \quad (15)$$

As also for the fixed bed condition the threshold $Q = 0.133$ L s^{-1} can be used (Figure 6), the following Γ_v expressions were obtained by

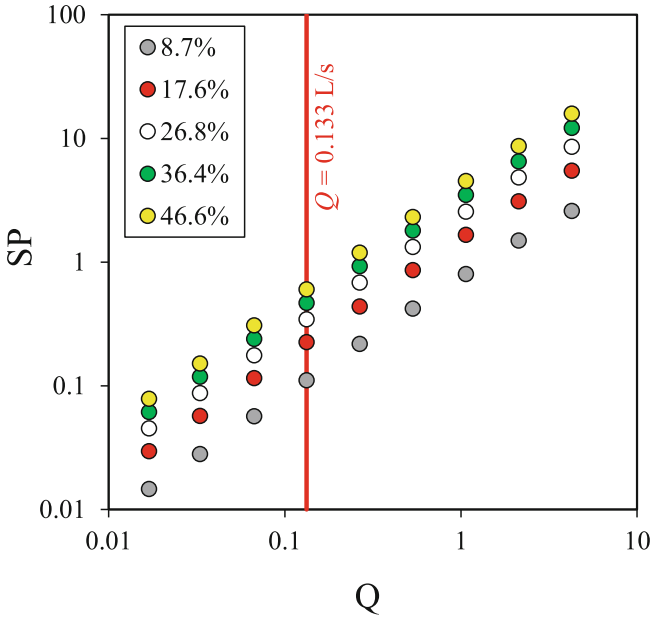

FIGURE 6 Relationship between flow discharge Q and stream power SP for fixed bed rills.

two sub-dataset characterized by $Q \le 0.133$ L s^{-1} (20 data) and $Q > 0.133$ L s^{-1} (25 data):

$$\Gamma_v = 1.4854 \frac{F^{1.1541}}{s^{0.587} Re^{0.186}} \quad (Q \le 0.133 \text{ L s}^{-1}), \quad (16a)$$

$$\Gamma_v = 0.5952 \frac{F^{1.0783}}{s^{0.5696} Re^{0.0392}} \quad (Q > 0.133 \text{ L s}^{-1}), \quad (16b)$$

which are characterized by R^2 of 0.989 and 0.983, respectively. Figure 7a shows the comparison between the measured Γ_v values, obtained by Equation (4), and those calculated by Equations (16). Introducing Equations (16) into Equation (3), the following flow resistance equations are obtained:

$$f = 8 \left[\frac{(\delta+1)(\delta+2)}{2^{1-\delta} 4.4817} \right]^{\frac{2}{1+\delta}} \left[\frac{s^{0.587} Re^{0.186}}{1.4854 F^{1.1541}} \right]^{\frac{2}{1+\delta}} \quad (Q \le 0.133 \text{ L s}^{-1}), \quad (17a)$$

$$f = 8 \left[\frac{(\delta+1)(\delta+2)}{2^{1-\delta} 4.4817} \right]^{\frac{2}{1+\delta}} \left[\frac{s^{0.5696} Re^{0.0392}}{0.5952 F^{1.0783}} \right]^{\frac{2}{1+\delta}} \quad (Q > 0.133 \text{ L s}^{-1}). \quad (17b)$$

Figure 7b shows the comparison between the measured f values and those calculated by Equations (17), which are characterized by RMSE equal to 0.0011 and errors always falling within the error bands of ±10%. Introducing the δ mean value (0.208) into Equations (17), they become:

$$f = 0.7091 \frac{s^{0.9719} Re^{0.3077}}{F^{1.9108}} \quad (Q \le 0.133 \text{ L s}^{-1}), \quad (18a)$$

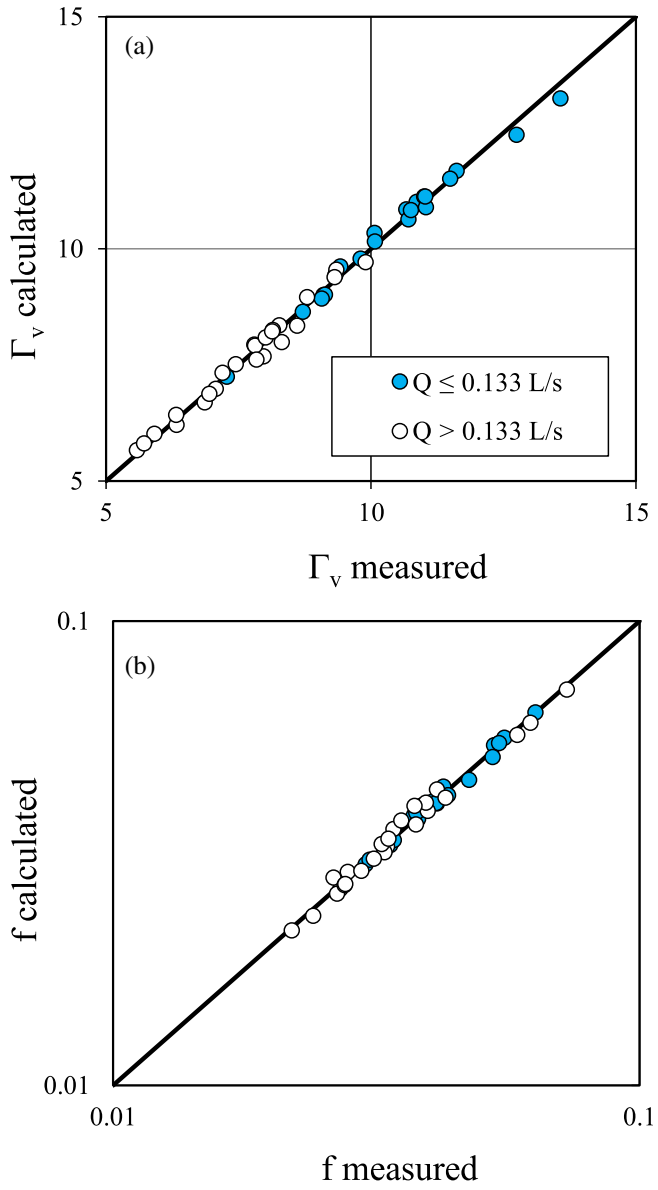

FIGURE 7 Comparison, for the fixed bed rills, between the measured Γ_v values, obtained by Equation (4), and those calculated by Equation (16a), and between the measured f values and those calculated by Equation (17b), distinguishing the data by the threshold $Q = 0.133$ L s^{-1}.

$$f = 3.2228 \frac{s^{0.943} Re^{0.0648}}{F^{1.7853}} \quad (Q > 0.133\,\text{L s} - 1). \tag{18b}$$

The fixed bed runs by Ban et al. (2020) were performed for rectangular rill cross-sections, which represent a simplification of the irregular shapes of natural rills. To investigate the possible effects due to the shape of the cross-sections, the applicability of the above relationships was tested for rills with irregular cross-sections. In particular, the data by Di Stefano, Nicosia, Palmeri, et al. (2019); Di Stefano et al. (2022b), obtained for fixed bed rills shaped on plots having slope gradients from 0.09 to 0.18, and 0.2 L s^{-1} ≤ Q ≤ 0.87 L s^{-1}, were used. To ensure the overlapping of the experimental conditions, Equation (17b), obtained for 0.087 ≤ s ≤ 0.466 and

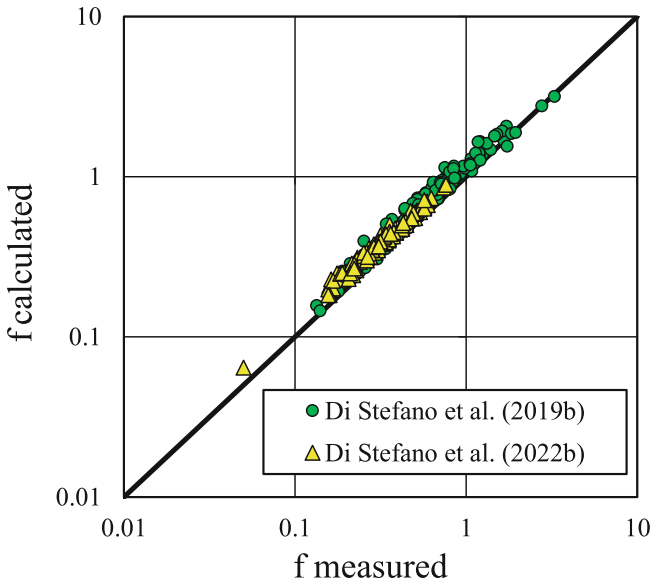

FIGURE 8 Comparison between the measured f values and those calculated by Equation (17b) for the testing dataset.

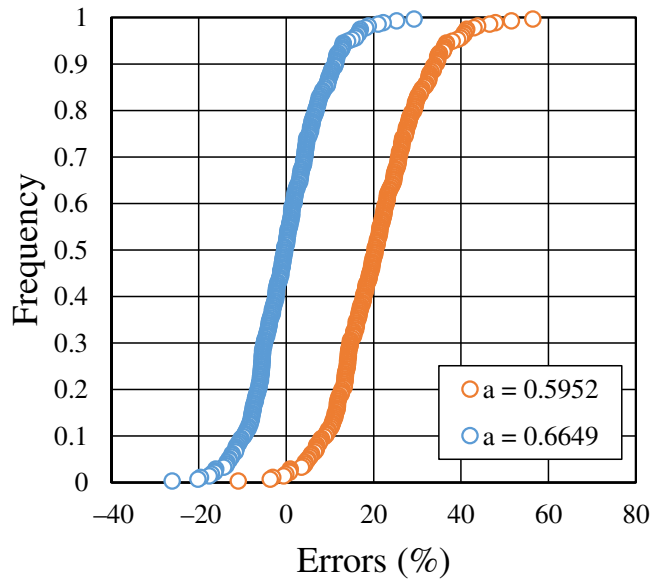

FIGURE 9 Empirical frequency distributions of the errors in the f estimate for the testing dataset obtained for different values of the a coefficient.

0.267 L s^{-1} ≤ Q ≤ 4.27 L s^{-1}, was tested. For the testing dataset, Figure 8 shows the comparison between the measured f values and those calculated by Equation (17b). This figure clearly highlights that Equation (17b) almost systematically overestimates f, with errors ranging from −11% to 56.4% (Figure 9) and falling within the error bands of ±20% and ±10% for the 48.3% and 11% of the examined cases, respectively. For this reason, the coefficients of Equation (17b) ($b = 1.0783$, $c = 0.5696$, and $e = 0.0392$) were fixed, and the Γ_v values were regressed against $X = \frac{F^{1.0783}}{s^{0.5696} Re^{0.0392}}$ (Figure 10) to determine the scale coefficient $a = 0.6649$ accounting for the shape of the cross-

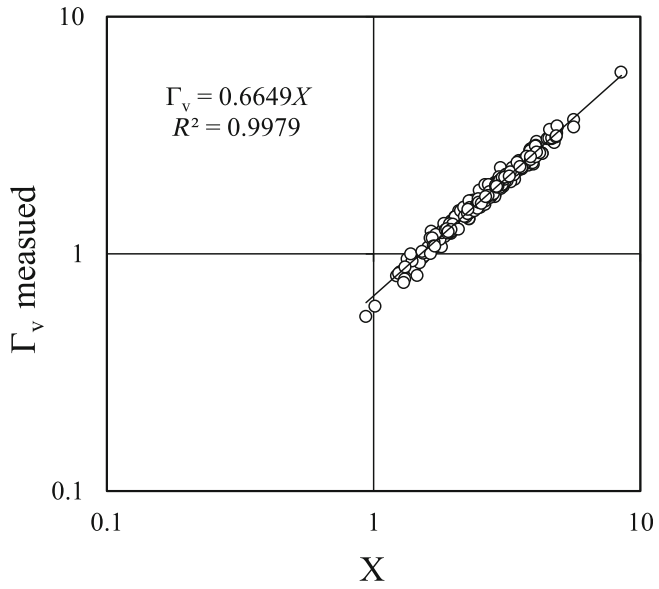

FIGURE 10 Plot of Γ_v versus X for the testing dataset by Di Stefano, Nicosia, Palmeri, et al. (2019); Di Stefano et al. (2022b).

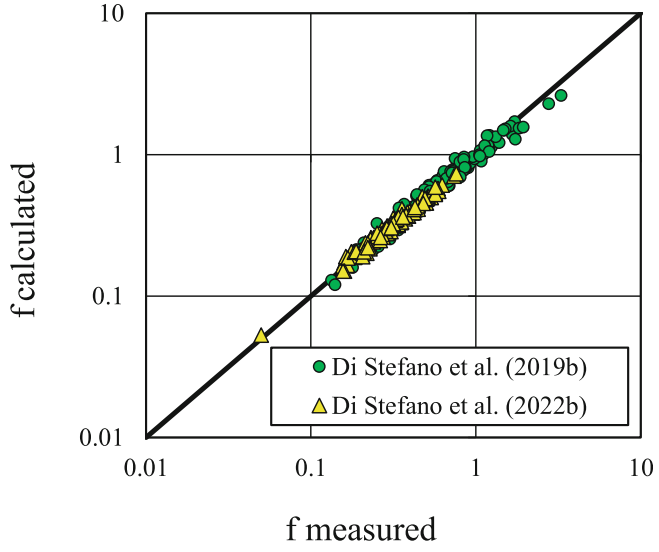

FIGURE 11 Comparison between the measured f values and those calculated by Equation (17b) with $a = 0.6649$ for the testing dataset.

sections. Figure 11 plots the comparison, for the testing dataset, between the measured f values and those calculated by Equation (17b) with $a = 0.6649$ in place of 0.5952. Using this scale coefficient significantly improves the f estimation, with errors ranging from −26% to 29% (Figure 9) and less than or equal to ±20% for 97.8% of cases and less than or equal to ±10% for 78% of cases.

4 | DISCUSSION

For both mobile (Figure 1a) and fixed (Figure 1b) bed conditions, Figure 1 shows that, for a given value of the Reynolds number, F increases with the slope gradient, especially for the fixed bed runs (Figure 1b). For fixed Re, hypothesizing the dependence between s and V, an increase of s should determine increasing mean flow velocities, decreasing water depths, and higher values of the Froude number, consequently. The comparison between Figure 1a, b demonstrates that the dependence between s and F is much more significant for the fixed bed runs than for the mobile bed ones, especially for turbulent flow regime. This result can be justified by the occurrence of the feedback mechanism for mobile bed rills characterized by turbulent flows and the absence of this mechanism for fixed bed rills. Moreover, Figure 1 highlights that, as expected, for fixed Reynolds number, the Froude number obtained for the mobile bed is significantly lower than that obtained for the fixed one. This result is due to the circumstance that, for given hydraulic conditions, the flow velocities on mobile beds are lower than those on the fixed ones as a rate of flow energy operates to detach and transport soil particles.

The accuracy of the Darcy–Weisbach friction factor estimate by Equations (8) (mobile bed) and (14) (fixed bed) calibrated using all the available data for a given bed condition, is not satisfactory if compared with that obtained by dividing the data with the threshold $Q = 0.133$ L s^{-1}. The improvements can be explained by the different flow behaviour in the two discharge ranges. Especially for low slope gradients, low discharges ($Q \leq 0.133$ L s^{-1}) imply low stream power and flow energy, consequently. The limit represented by this low energy is particularly marked for flow on mobile beds, for which an energy rate has to be used for sediment detachment and transport. On the contrary, for discharges higher than 0.133 L s^{-1}, the flow has more energy for its motion (fixed and mobile beds) and erosive phenomena (mobile bed).

Moreover, the improvements in the model performance, applying this threshold, are more evident for the mobile bed condition. This result is probably due to the circumstance that, for mobile beds, the relationships between the stream power and the sediment transport capacity (Ferro, 1998) and detachment capacity have to be considered. The investigated soil has a silt loam texture (25.62% sand, 64.57% silt, and 9.81% clay), and is characterized by high detachability and medium-low transportability. Consequently, for the investigated soil, the limiting factor is the transport capacity rather than the detachment capacity. Low stream powers, determined by low values of discharge and slope gradient, determine low sediment transport capacity, which becomes a limiting factor, as suggested by Nicosia et al. (2022). These authors, investigating the slope effects on rill erosion phenomena, found that, for steep slopes, the sediment transport capacity is so high that it is not a limiting factor for the actual sediment transport, while, for gentle slopes, the actual sediment transport could be limited by both T_c and the detachability and transportability characteristics of the soil particles. This result can be confirmed by the fact that, only for the mobile bed runs, for which sediment transport phenomena occur, the obtained exponents of the Reynolds number have opposite signs (Equations (11a) and (11b)). This finding can be justified by the fact that, for the investigated soil, the chosen threshold ($Q = 0.133$ L s^{-1}) implies a discrimination between a negligible sediment transport (i.e., the hydraulic behaviour of the mobile

bed rills is similar to that of the fixed ones) and a relevant sediment transport for $Q > 0.133$ L s^{-1}.

Finally, for mobile bed rills, Equations (12) show that the exponent of s is far from 1 (0.7) for $Q \leq 0.133$ L s^{-1}, while it is close to 1 (0.8924) for $Q > 0.133$ L s^{-1}. According to Chezy's equation, when the Darcy–Weisbach friction factor is linearly related to s (i.e., its exponent is approximately 1), the flow velocity is independent of the channel slope. Consequently, according to the obtained results, the 'feedback mechanism' presented by Govers (1992) tends to occur for $Q > 0.133$ L s^{-1}. These results do not agree with the statement by Ban (2023) regarding the slope independence of flow velocity for Q less than or equal to 0.133 L s^{-1}. For $Q \leq 0.133$ L s^{-1}, the sediment transport phenomena are negligible and, consequently, the rill can be considered as a fixed bed channel. In this case, the dependence of flow velocity on the channel slope should occur, as found by Foster et al. (1984). On the contrary, for $Q > 0.133$ L s^{-1}, the erosive phenomena are relevant, and the increase of V with s is counterbalanced by the increased roughness.

On the other hand, the s exponent into Equations (18) (0.94 for $Q \leq 0.133$ L s^{-1}, and 0.97 for $Q > 0.133$ L s^{-1}) for fixed beds, is close to 1. However, this result cannot be explained by the feedback mechanism, and could be affected by uncertainties on the velocity measurement due to the flow instability and self-aeration phenomena that characterize supercritical flows with high Froude numbers (Montuori, 1984), as those used in the investigation by Ban et al. (2020) ($3.8 \leq F \leq 10.8$) (Figure 1b).

At last, the analysis developed on the testing dataset, constituted by the measurements performed for fixed bed rills by Di Stefano, Nicosia, Palmeri, et al. (2019) and Di Stefano et al. (2022b), demonstrated that the effects of the cross-section shape on flow resistance are not negligible. In fact, for given experimental conditions (i.e., comparable ranges of s and Q), the coefficient a (0.5592), obtained for rills with rectangular cross-sections, leads to overestimate the Darcy–Weisbach friction factor for rills with irregular cross-sections but its change is sufficient to delete the prediction bias.

The main limitation of the developed analysis is that the applied threshold could not be valid for a different soil. A future study, focused on the effects of the soil texture on the threshold value, could be developed. Another limitation of this study is that, for mobile bed rills, the water depth values were calculated considering a constant w value, neglecting the shaping effect of the flow on rill geometry.

5 | CONCLUSIONS

For both the mobile and fixed bed conditions, the analysis was performed, at first, considering all the available data and then splitting these data by a threshold $Q = 0.133$ L s^{-1}, which can be used to divide the database as it determines two tendentially distinguished stream power ranges.

The accuracy of the Darcy–Weisbach friction factor estimate improved considering the abovementioned threshold, confirming that differences in flow behaviour occur for different ranges of stream power, which is governed by discharge and slope gradient.

For mobile bed conditions, the feedback mechanism does not occur for discharge values lower than or equal to 0.133 L s^{-1}, as the sediment transport phenomena are negligible, and rills can be considered as fixed bed channels. Oppositely, when the erosive phenomena are significant ($Q > 0.133$ L s^{-1}), the feedback mechanism tends to occur due to the change of bed roughness depending on slope, confirming that flow resistance is influenced by the rill flow-sediment transport interaction.

For the fixed bed rills, the obtained exponents of the slope gradient cannot be justified by the feedback mechanism, but they could be due to uncertainties in the velocity measurement caused by the flow instability and self-aeration phenomena characterizing supercritical flows with high Froude numbers.

The results also showed that the effects of the cross-section shape on flow resistance are significant, as rectangular and irregular cross-sections require different scale coefficients a.

ACKNOWLEDGEMENTS

All authors set up the research, analysed and interpreted the results and contributed to write the paper. This research did not receive any specific grant from funding agencies in the public, commercial, or not-for-profit sectors.

CONFLICT OF INTEREST STATEMENT

The authors declare that they have no known competing financial interests or personal relationships that could have appeared to influence the work reported in this paper.

DATA AVAILABILITY STATEMENT

Data sharing not applicable to this article as no datasets were generated or analysed during the current study.

ORCID

Alessio Nicosia https://orcid.org/0000-0003-0540-8788
Vincenzo Pampalone https://orcid.org/0000-0002-5195-9209
Vito Ferro https://orcid.org/0000-0003-3020-3119

REFERENCES

Ali, M., Seeger, M., Sterk, G., Seeger, M., Boersema, M. P., & Peters, P. (2013). A unit stream power based sediment transport function for overland flow. *Catena*, *101*, 197–204.

Bagarello, V., & Ferro, V. (2004). Plot-scale measurements of soil erosion at the experimental area of Sparacia (southern Italy). *Hydrological Processes*, *18*, 141–157.

Ban, Y. Y. (2023). Measurements and estimation of flow velocity in mobile bed rills. *International Journal of Sediment Research*, *38*(1), 97–104. https://doi.org/10.1016/j.ijsrc.2022.07.003

Ban, Y. Y., Wang, W., & Lei, T. W. (2020). Measurement of rill and ephemeral gully flow velocities and their model expression affected by flow rate and slope gradient. *Journal of Hydrology*, *589*, 125172. https://doi.org/10.1016/j.jhydrol.2020.125172

Barenblatt, G. I. (1979). *Similarity, self-similarity, and intermediate Asymptotics* (p. 218). Consultants Bureau Plenum Press.

Barenblatt, G. I. (1987). *Dimensional analysis*. Gordon & Breach, Science Publishers Inc.

Borrelli, P., Robinson, D. A., Fleischer, L. R., Lugato, E., Ballabio, C., Alewell, C., Meusburger, K., Modugno, S., Schutt, B., Ferro, V., Bagarello, V., Van Oost, K., Montanarella, L., & Panagos, P. (2017). An assessment of the global impact of the 21st century land use change on soil erosion. *Nature Communications*, *8*, 1–13.

Carollo, F. G., Di Stefano, C., Nicosia, A., Palmeri, V., Pampalone, V., & Ferro, V. (2021). Flow resistance in mobile bed rills shaped in soils with different texture. *European Journal of Soil Science*, *72*, 2062–2075.

Castaing, B., Gagne, Y., & Hopfinger, E. J. (1990). Velocity probability density functions of high Reynolds number turbulence. *Physica D: Nonlinear Phenomena*, *46*, 177–200.

Di Stefano, C., Nicosia, A., Palmeri, V., Pampalone, V., & Ferro, V. (2019). Comparing flow resistance law for fixed and mobile bed rills. *Hydrological Processes*, *33*, 3330–3348. https://doi.org/10.1002/hyp.13561

Di Stefano, C., Nicosia, A., Palmeri, V., Pampalone, V., & Ferro, V. (2020). Flow resistance law under suspended sediment laden conditions. *Flow Measurement and Instrumentation*, *74*, 101771. https://doi.org/10.1016/j.flowmeasinst.2020.101771

Di Stefano, C., Nicosia, A., Palmeri, V., Pampalone, V., & Ferro, V. (2021). Estimating flow resistance in steep slope rills. *Hydrological Processes*, *35*(7), e14296. https://doi.org/10.1002/hyp.14296

Di Stefano, C., Nicosia, A., Palmeri, V., Pampalone, V., & Ferro, V. (2022a). Rill flow velocity and resistance law: A review. *Earth Science Reviews*, *231*, 104092. https://doi.org/10.1016/j.earscirev.2022.104092

Di Stefano, C., Nicosia, A., Palmeri, V., Pampalone, V., & Ferro, V. (2022b). Rill flow resistance law under sediment transport. *Journal of Soils and Sediments*, *22*, 334–347. https://doi.org/10.1007/s11368-021-03083-x

Di Stefano, C., Nicosia, A., Pampalone, V., Palmeri, V., & Ferro, V. (2019). Rill flow resistance law under equilibrium bed-load transport conditions. *Hydrological Processes*, *33*, 1317–1323.

Everaert, W. (1991). Empirical relations for the sediment transport capacity of interrill flow. *Earth Surface Processes and Landforms*, *16*, 513–532.

Ferro, V. (1998). Evaluating overland flow sediment transport capacity. *Hydrological Processes*, *12*, 1895–1910.

Ferro, V. (2017). New flow resistance law for steep mountain streams based on velocity profile. *Journal of Irrigation and Drainage Engineering*, *143*, 1–6.

Ferro, V. (2018). Assessing flow resistance in gravel bed channels by dimensional analysis and self-similarity. *Catena*, *169*, 119–127.

Ferro, V., & Porto, P. (2018). Applying hypothesis of self-similarity for flow resistance law in Calabrian gravel bed rivers (Fiumare). *Journal of Hydraulic Engineering*, *144*, 1–11.

Foster, G. R., Huggins, L. F., & Meyer, L. D. (1984). A laboratory study of rill hydraulics: I velocity relationships. *Transactions of the ASAE*, *27*, 790–796.

Gao, P., & Abrahams, A. D. (2004). Bedload transport resistance in rough open-channel flows. *Earth Surface Processes and Landforms*, *29*, 423–435.

Govers, G. (1990). Empirical relationships for the transport capacity of overland flow, transport and deposition processes, proceedings of the Jerusalem workshop. *IAHS Publication*, *189*, 45–63.

Govers, G. (1992). Relationship between discharge, velocity and flow area for rills eroding loose, non-layered materials. *Earth Surface Processes and Landforms*, *17*, 515–528.

Govers, G., Gimenez, R., & Van Oost, K. (2007). Rill erosion: Exploring the relationship between experiments, modeling and field observations. *Earth Science Reviews*, *8*, 87–102.

Jiang, F., Gao, P., Si, X., Zhan, Z., Zhang, H., Lin, J., Ji, X., Wang, M. K., & Huang, Y. (2018). Modelling the sediment transport capacity of flows in nonerodible rills. *Hydrological Processes*, *32*, 3852–3865.

Li, P., Zhang, K., Wang, J., Meng, H., Nicosia, A., & Ferro, V. (2022). Overland flow hydrodynamic characteristics in rough beds at low Reynolds numbers. *Journal of Hydrology*, *607*, 127555. https://doi.org/10.1016/j.jhydrol.2022.127555

Montuori, C. (1984). *Sviluppi recenti nello studio delle correnti supercritiche. Dipartimento di Idraulica, Gestione delle Risorse Idriche ed Ingegneria Ambientale, Memoria 508*. Università: Napoli (in Italian).

Nearing, M. A., Norton, L. D., Bulgakov, D. A., Larionov, G. A., West, L. T., & Dontsova, K. M. (1997). Hydraulics and erosion in eroding rills. *Water Resources Research*, *33*, 865–876.

Nicosia, A., & Ferro, V. (2023). Flow resistance due to shrubs and woody vegetation. *Flow Measurement and Instrumentation*, *89*, 102308. https://doi.org/10.1016/j.flowmeasinst.2023.102308

Nicosia, A., Palmeri, V., Pampalone, V., Di Stefano, C., & Ferro, V. (2022). Slope threshold in rill flow resistance. *Catena*, *208*, 105789. https://doi.org/10.1016/j.catena.2021.105789

Nouwakpo, S. K., Williams, C. J., Al-Hamdam, O. Z., Weltz, M. A., Pierson, F., & Nearing, M. (2016). A review of concentrated flow erosion processes on rangelands: Fundamental understanding and knowledge gaps. *International Soil and Water Conservation Research*, *4*, 75–86.

Peng, W., Zhang, Z., & Zhang, K. (2015). Hydrodynamic characteristics of rill flow on steep slopes. *Hydrological Processes*, *29*, 3677–3686.

Strohmeier, S. M., Nouwakpo, S. K., Huang, C. H., & Klik, A. (2014). Flume experimental evaluation of the effect of rill flow path tortuosity on rill roughness based on the Manning-Strickler equation. *Catena*, *118*, 226–233. https://doi.org/10.1016/j.catena.2014.01.011

Wang, Z., Yang, X., Liu, J., & Yuan, Y. (2015). Sediment transport capacity and its response to hydraulic parameters in experimental rill flow on steep slope. *Journal of Soil and Water Conservation*, *70*(1), 36–44.

Wirtz, S., Seeger, M., & Ries, J. B. (2010). The rill experiment as a method to approach a quantification of rill erosion process activity. *Zeitschrift für Geomorphologie*, *54*, 47–64.

Wu, B., Wang, Z. L., Shen, N., & Wang, S. (2016). Modelling sediment transport capacity of rill flow for loess sediments on steep slopes. *Catena*, *147*, 453–462.

Yang, C. T. (1972). Unit stream power and sediment transport. *Journal of the Hydraulics Division*, *98*(10), 1805–1826.

Zhang, G. H., Liu, Y. M., Han, Y. F., & Zhang, X. H. (2009). Sediment transport and soil detachment on steep slopes: I. transport capacity estimation. *Soil Science Society of America Journal*, *73*(4), 1291–1297.

How to cite this article: Nicosia, A., Pampalone, V., Serio, M. A., & Ferro, V. (2023). Evaluating the effects of stream power on rill flow resistance. *Hydrological Processes*, *37*(6), e14930. https://doi.org/10.1002/hyp.14930